Counter flow microbubble channeling using acoustic radiation force funnel

Benjamin Raiton, James R. McLaughlan, Peter R. Smith, David M. J. Cowell, Sevan Harput and Steven Freear
Ultrasound Group, School of Electronic and Electrical Engineering, University of Leeds.

***Abstract*—Acoustic radiation force has become a significant factor in the research to enhance the targeting of microbubbles for molecular imaging and drug delivery. In this study microbubbles are flown through an opposing radiation force funnel and the impact on their path is compared to the theory. The experiments demonstrate that the behavior of the lipid microbubbles is in accordance with the simulation. Although the force required to stop microbubbles flowing at 10 mm/s is in the order of 100s of nN, large clusters are successfully held against the flow.**

I. Introduction

Several biomedical applications are significantly benefiting from the use of acoustic radiation force (ARF) such as targeted molecular imaging [1] and targeted drug or gene delivery [2]. By pushing microbubbles (MBs) away from circulation and toward the endothelium, the ligand-receptor gap can be reduced hence enhancing targeting efficiency [3]. There exist different approaches to apply sufficient force onto a particle to promote a controllable and repeatable translation. Either with ultrasound through the generation of standing-waves [4], micro-beams [5], or by employing optical-tweezers [6]. Yet, due to the need for high frequencies or small working distances, none of these techniques can be applied *in-vivo* [7]. Only ultrasound traveling waves are suitable when the region of interest is located deep within the human body.
One of the first publications on the generation of a pressure null using traveling waves was in 1998 by Yamakoshi *et al.* [8]. Since then this group has published several studies employing the same principle [9], [10]. However, this approach is limited as the source is made up of only two focused single element transducers. The setup presented here exploits the flexibility given by one-dimensional medical probes. The aim of this study is to verify if the behavior of a standard distribution of lipid microbubbles near the pressure null complies with existing theory. The generation of a pressure cancellation using traveling waves induces an axial radiation force as well as a lateral trapping force due to the pressure gradient, both of which are considered in this study.

II. Radiation Force

A. Primary Radiation Force

For a traveling plane wave and assuming the microbubbles are much smaller than the wavelength, the primary radiation force (PRF) can be expressed as [11]:

$$F_{PRF} = \frac{2\pi P_A^2 \alpha\, r_0}{\rho_0\, c\, \omega} \frac{2\beta_{tot}/\omega}{\{(\omega_0/\omega)^2 - 1\}^2 + \{2\beta_{tot}/\omega\}^2} \quad (1)$$

where $\beta_{tot} = \delta_{tot}\omega_0/2$ is the dimensionless damping coefficient. The excitation pulsation is noted $\omega = 2\pi f$ while the microbubble resonance pulsation is $\omega_0 = 2\pi f_0$. For simplicity, the microbubble radius r_0 is assumed to be constant when calculating the PRF. For the other variables please refer to Table I.

B. Trapping Force

Particle manipulation using standing waves rests on the primary Bjerknes force principle. According to Leighton *et al.* [12], microbubbles excited below resonance will travel up a pressure gradient yet those above resonance will travel in the other direction. In the same publication they also indicate that this theory is valid in any field containing a pressure gradient. For a MB of constant volume $V_0 = 4\pi\ r_0^3/3$ subject to a pressure gradient ∇P, the average acoustic trapping force (TF) is:

$$F_{TF} = -V_0 \langle \nabla P(r,t) \rangle \quad (2)$$

C. Drag Force

As the ultrasound pressure wavefront propagates in the opposite direction to the fluid, the drag force is calculated to evaluate if the PRF is expected to alter the flowing direction of the microbubbles. In the case of laminar flow and for a MB flowing at a velocity v_b within a Newtonian fluid of velocity v_f, the drag force (DF) is [13]:

$$F_D = \frac{3}{2}\pi r_0 \eta \rho \frac{C_D R_e}{24} ||v_f - v_b|| \quad (3)$$

where η and ρ are the fluid viscosity and density respectively. $R_e = ||v_f - v_b||/\eta$ is the Reynolds number while C_D is the drag coefficient. The equilibrium point of these forces can be calculated for a single microbubble with equations (1) and (3) by setting $v_b = 0$ and solving $F_{PRF} = F_D$.

III. Methods

A. Simulations

1) Primary Radiation Force: To graphically evaluate if MB will change course once the ultrasound is applied, the primary radiation force and drag force are plotted with MATLAB (Mathworks Inc., Natick, MA, USA) using the values given in Table I. As the fluid velocity is expected to be lower near the vessel walls, F_D is also plotted for reduced values of v_f. Any microbubbles for which the condition $F_{PRF} > F_D$ is verified should see their flowing direction

Definition	Symbol	Value
Radius	r_0	1 μm
Polytropic exponent	γ	1.06
Water density	ρ	1000 kg/m^3
Water viscosity	η	0.001 Pa.s
Acceleration	g	9.8 m/s
Shell stiffness	S_p	1.88 N/m
Shell friction	S_f	0.09 mg/s
Ambient pressure	p_0	100 kPa
Water velocity	c	1500 m/s
Number of elements	n_{el}	96
Center frequency	f_{TD}	4.8 MHz
Bandwidth	B	57%
Pitch	p	304.8 μm
Element eight	h	6 mm
Excitation frequency	f	5 MHz
Pulsing ratio	α	0.4
Acoustic pressure	P_A	1.8 MPa
Focal depth	z_f	30 mm

TABLE I
MICROBUBBLE (TOP) AND LINEAR ARRAY (BOTTOM) PARAMETERS

reversed.

2) Trapping Force: The Field II package [14], [15] is first used to simulate the pressure field at the focal depth z_f. The simulation parameters listed in Table I are chosen to replicate the experiments. The pressure field $P(x,t)$ is then extracted for $y = 0$, $z = z_f$ and x varying from -0.5 mm to 0.5 mm, see Figure 1 for axis orientation. Finally the trapping force is calculated using equation (2).

B. Hydrophone Measurements

Before performing the experiments with the microbubbles, the pressure field is first validated using a hydrophone. This is to confirm the existence of the pressure cancellation and to evaluate the amount of nonlinearity at the focal depth. A one-dimensional medical ultrasound array (L3-8/40EP Prosonic, Korea) is aligned with a 0.2 mm needle hydrophone (Precision Acoustics Ltd., Dorchester, UK) at a distance z_f within a tank of de-ionized and de-gassed water at 20°C $\pm$1°C. The hydrophone is mounted on a 3-D computer controlled translation system to acquire a lateral scan from $x = -0.5$ mm to 0.5 mm, with 0.1 mm steps. The signal is digitized by a LeCroy 64xi digital oscilloscope (LeCroy Corporation, Chestnut Ridge, NY, USA). The data is then processed in MATLAB on a personal computer, and averaged over five consecutive measurements. The lateral plot is obtained both with and without phase inversion. In the latter case, the fast Fourier transform (FFT) is computed to get a measure of the nonlinearity at the focal depth by examining the second and third harmonics. The fourth harmonic and above are not taken into account as the hydrophone is only calibrated up to 20 MHz. Since it is expected to be within the shock-free regime for $\sigma < 1$, the Fubini solution can be applied [16]:

$$B_n = \frac{2}{n\sigma} J_n(n\sigma) \tag{4}$$

where B_n is the relative magnitude of the harmonic of order n and J_n the Bessel function.

C. Experiments

1) Ultrasound Array Research Platform: Commercial ultrasound imaging equipment are not suitable for radiation force applications [17]. For that reason, the bespoke Ultrasound Array Research Platform (UARP) was designed by the Ultrasound Group at the University of Leeds [18]. 96 elements of the array are focused at the same depth z_f and are transmitting an identical tone burst. The only variation compared to a standard beam is that both halves of the array are out of phase by π (see Figure 1). This results in the mixing of the two opposite-phase pressure fields along the depth z aligned with the center of the array for $x = 0$.

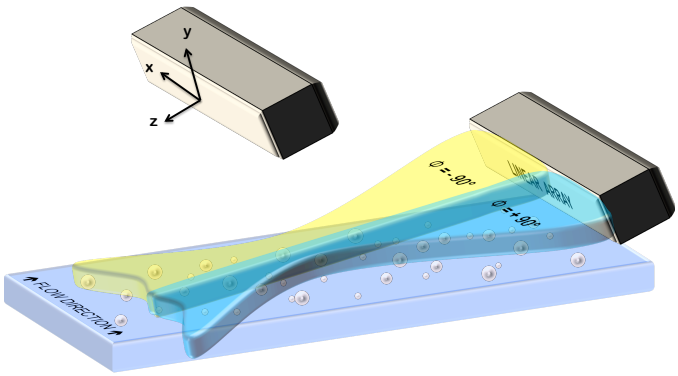

Fig. 1. Experimental Setup illustrating opposite-phase fields and position of the linear array in relation to the Ibidi slide. Flow direction: left to right.

2) Experimental Setup: The lipid microbubbles have a size distribution of 1 to 10 μm, with the majority of the MB population found around 2 μm. Their shell stiffness and friction parameters were experimentally measured to be S_p=1.88 N/m and S_f=0.09 mg/s respectively. The MBs are diluted to a ratio of 1:1000 and circulated in de-gassed water at 20°C $\pm$1°C, through the center channel of a μ-Slide III (Ibidi μ-slide, Ibidi, Martinsried, Germany) and maintained at a constant flow rate by using a programmable syringe pump. The flow channel is 1 mm wide and 100 μm deep. An inverted microscope (Eclipse T*i*-U, Nikon, Melville, NY, USA) is located directly underneath the slide for optical observations. The orientation of the linear array in relation to the slide is illustrated in Figure 1.

IV. RESULTS AND DISCUSSION

A. Simulations

1) Primary Radiation Force: As established from the hydrophone measurements, and for the conditions listed in Table I, the peak negative pressure reaches 1.8 MPa within the two mainlobes. Figure 2 shows that, at this pressure, and for a transmitting frequency of 5 MHz, the primary radiation force peaks at 2 μN. The maximum is reached for microbubbles that

have a radius of 1.63 μm as this corresponds to a resonant frequency $f_0 = 5$ MHz. For a maximum fluid velocity of 10 mm/s, only a section of the MB population is affected by the PRF. Whereas, at a reduced velocity of 1 mm/s, the majority of the MBs should see their trajectory reversed. Near the vessel wall, where v_f is minimum, the $F_{PRF} > F_D$ condition is verified for the whole microbubble population. In fact, extending the simulation for $r_0 > 10$ μm, reveals that even clusters should travel against the flow, as long as they remain near a boundary.

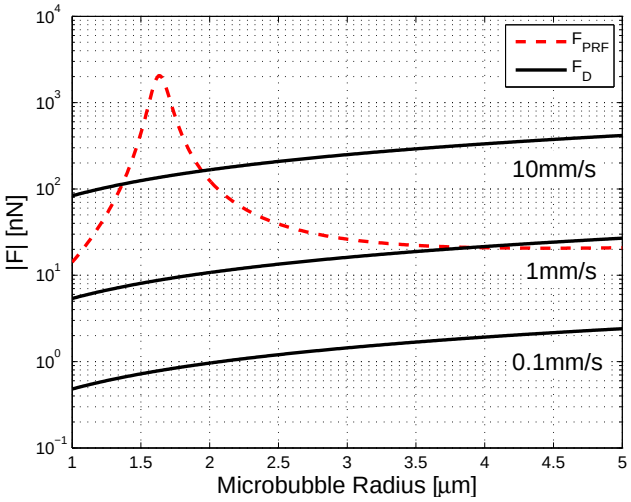

Fig. 2. Simulation of DF (continuous line) and PRF (dashed line) as seen by a single bubble of varying radius

2) Trapping Force: The trapping force profile displayed in Figure 3 is normalized so that it is independent of the MB size. As F_{TF} is proportional to r_0^3, larger bubbles are subject to a greater trapping force. As demonstrated in Figure 2, microbubbles that are resonant at 5 MHz have a radius of 1.63 μm. Hence, according to the primary Bjerknes force, small MBs excited below resonance are attracted to the two pressure peaks. On the other hand, microbubbles of radius $r_0 >$1.63 μm are affected by the trapping force and align at the center of the funnel. Although, due to the pressure cancellation, the PRF will not be sufficient to reverse the flowing direction of the larger trapped microbubbles. According to the simulated pressure field, the two peaks are spaced 260 μm away from the funnel center.

B. Experiments

1) Pressure Field: The UARP system is first setup to transmit a non-inverted beam. Figure 4 is the FFT of the measured signal at the focal point.The plot is normalized to the fundamental at 5 MHz. The second harmonic level is measured at -11.1 dB and the third harmonic at -17.8 dB. According to (4), σ = 0.65 which is within the weakly nonlinear regime as expected. The lateral plot on Figure 5 confirms that there is a pressure cancellation for x = 0, and the gap between the funnel axis and sidelobes is in accordance with the simulation. One might notice that the pressure cancellation is not ideal with

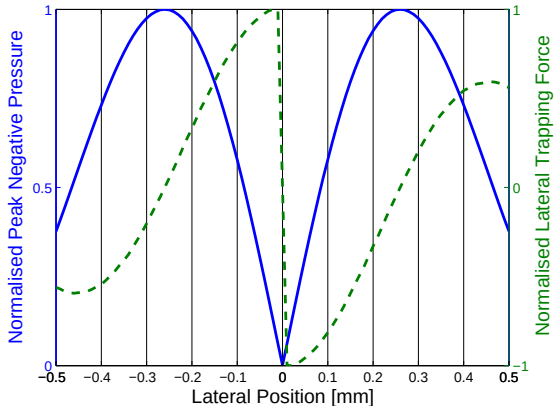

Fig. 3. Simulation of the normalised pressure field (continuous line) and trapping force (dashed line)

the normalized PNP minimum at 0.15. This is put down to the fact that the diameter of the hydrophone is 200 μm which is relatively large in relation to the funnel lateral dimensions.

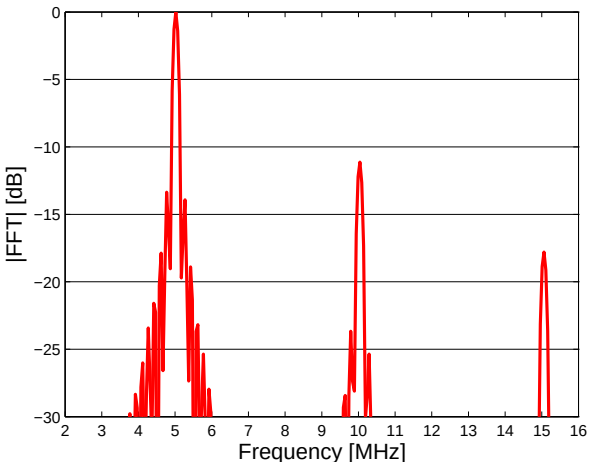

Fig. 4. FFT at focal point for non-inverted beam

2) Channel formation: The scale displayed on Figure 6 reveals a channel spacing of $\pm$250 μm which agrees with the simulation and the lateral pressure plot of Figure 5. The experiment also confirms that the PRF is lower within the center channel, at the pressure null as MBs don't see their flowing direction affected. Clusters are clearly formed inside the other two channels where the pressure is of greater magnitude yielding a stronger secondary radiation force [11]. Furthermore, the PRF exerted onto these aggregated MBs is sufficient to stop their flow. The minimum angle between the array and the Ibidi slide, due to experimental setup restrictions, means that F_{PRF} isn't directly opposing F_D. This explains why the flowing direction of clusters within the two side channels cannot be successfully reversed. Overall the behavior of the MB distribution flowing through the acoustic funnel is in accordance with the simulation.

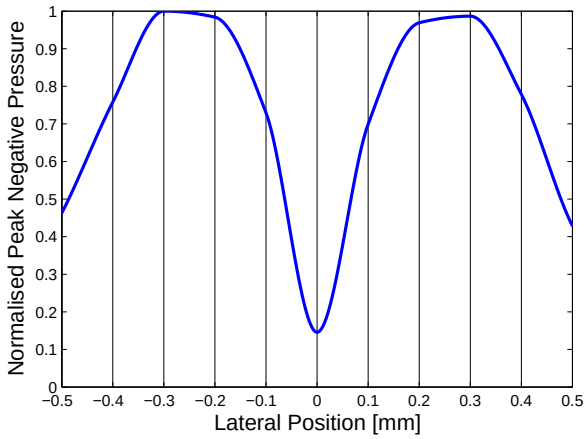

Fig. 5. Normalised hydrophone measurement of the lateral pressure plot

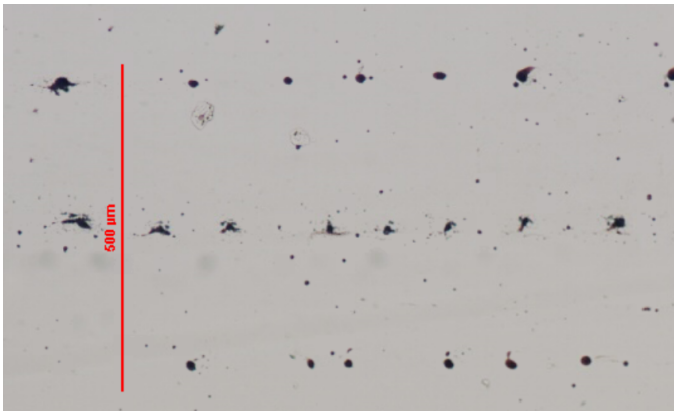

Fig. 6. Microscope observation using 10x objective. Ultrasound beams propagating from right to left opposing the flow direction.

V. Conclusion

In this study we demonstrated that the behavior of 1-10 μm lipid microbubbles flowing through an acoustic radiation force funnel is in accordance with the simulation. It is also interesting to note the magnitude of the force required to completely stop flowing microbubbles even for a relatively low velocity. Future work could lead to the study of the MB size distribution within each channel. According to the primary Bjerknes force only MBs excited above resonance should be flowing along the pressure null.

VI. Acknowledgment

The author would like to thank the Royal Academy of Engineering and Elster Instromet for their support.

References

[1] R. Gessner and P. A. Dayton, "Advances in molecular imaging with ultrasound," *Mol Imaging*, vol. 9, pp. 117–127, 2010.

[2] S. C. D. S. Ine Lentacker and N. N. Sanders, "Drug loaded microbubble design for ultrasound triggered delivery," *Soft Matter*, vol. 5, pp. 2161–2170, 2009.

[3] B. J. Schmidt, I. Sousa, A. A. van Beek, and M. R. Bohmer, "Adhesion and ultrasound-induced delivery from monodisperse microbubbles in a parallel plate flow cell," *Journal of Controlled Release*, vol. 131, no. 1, pp. 19–26, 2008.

[4] S. Oberti, D. Moller, A. Neild, J. Dual, F. Beyeler, B. J. Nelson, and S. Gutmann, "Strategies for single particle manipulation using acoustic and flow fields," *Ultrasonics*, vol. 50, no. 2, pp. 247–257, 2010, selected Papers from ICU 2009.

[5] J. Lee, C. Lee, and K. Shung, "Calibration of sound forces in acoustic traps," *IEEE Trans. UFFC*, vol. 57, no. 10, pp. 2305–2310, 2010.

[6] P. H. Jones, E. Stride, and N. Saffari, "Trapping and manipulation of microscopic bubbles with a scanning optical tweezer," *Applied Physics Letters*, vol. 89, no. 081113, pp. 1–3, 2006.

[7] S.-T. Kang and C.-K. Yeh, "Potential-well model in acoustic tweezers," *IEEE Trans. UFFC*, vol. 57, no. 6, pp. 1451–1459, 2010.

[8] Y. Yamakoshi and Y. Noguchi, "Micro particle trapping by opposite phases ultrasonic travelling waves," *Ultrasonics*, vol. 36, no. 8, pp. 873–878, 1998.

[9] Y. Yamakoshi and T. Miwa, "Micro bubble adhesion to target wall by frequency sweep of ultrasonic pumping wave," in *IEEE Ultrasonics Symposium (IUS)*, 2008, pp. 345–348.

[10] Y. Yamakoshi, T. Miwa, N. Yoshizawa, Y. Takahashi, and H. Inoguchi, "Effect of pre-trapping of micro bubbles on mechanical damage enhancement in bubble cavitation," in *IEEE Ultrasonics Symposium (IUS)*, 2009, pp. 1270–1273.

[11] P. Dayton, K. Morgan, A. Klibanov, G. Brandenburger, K. Nightingale, and K. Ferrara, "A preliminary evaluation of the effects of primary and secondary radiation forces on acoustic contrast agents," *Ultrasonics, Ferroelectrics and Frequency Control, IEEE Transactions on*, vol. 44, no. 6, pp. 1264–1277, 1997.

[12] T. G. Leighton, A. J. Walton, and M. J. W. Pickworth, "Primary bjerknes forces," *European Journal of Physics*, vol. 11, no. 1, pp. 47–50, 1990.

[13] J.-M. Girault, D. Kouame, S. Menigot, G. Souchon, and F. Tranquart, "Analysis of index modulation in microembolic doppler signals part i: Radiation force as a new hypothesis-simulations," *Ultrasound in Medicine and Biology*, vol. 37, no. 1, pp. 87–101, 2011.

[14] J. Jensen and N. Svendsen, "Calculation of pressure fields from arbitrarily shaped, apodized, and excited ultrasound transducers," *Ultrasonics, Ferroelectrics and Frequency Control, IEEE Transactions on*, vol. 39, no. 2, pp. 262–267, 1992.

[15] J. A. Jensen, "Field: A program for simulating ultrasound systems," in *10th Nordicbaltic Conference on Biomedical Imaging, Vol. 4, no. 1*, 1996, pp. 351–353.

[16] D. T. Blackstock, "Connection between the fay and fubini solutions for plane sound waves of finite amplitude," *J. Acoust. Soc. Am.*, vol. 39, no. 6, pp. 1019–1026, 1966.

[17] R. Gessner, M. Lukacs, M. Lee, J. Tsuruta, F. Foster, and P. Dayton, "Radiation force-enhanced targeted imaging and near real-time molecular imaging using a dual-frequency high-resolution transducer: In-vitro and in-vivo results," in *Ultrasonics Symposium (IUS), 2009 IEEE International*, 2009, pp. 9–12.

[18] P. R. Smith, D. M. J. Cowell, B. Raiton, C. V. Ky, T. H. Pham, B. Q. Bui, and S. Freear, "A pll-based phased array method to minimize phase quantization errors and reduce phasing-lobes," in *IEEE Ultrasonics Symposium (IUS)*, 2010, pp. 1837–1840.